Digital Holography applied to simultaneously measure the shape and the radial deformation of a blood vessel (ex-vivo)

Nieves Andrés*, Cristina Pinto, Julia Lobera, Ana Mª López, Virginia Palero and M. Pilar Arroyo

Aragon Institute of Engineering Research (I3A), Facultad de Ciencias, Zaragoza University. c/ Pedro Cerbuna, 12, 50009 Zaragoza .

Abstract: Radial deformation of blood vessels has been measured by combining shape and deformation measurements. The difficulty of measuring both magnitudes simultaneously is related to the different order of magnitude. The veins have diameters up to 20 mm and suffer micrometric deformations due to cardiac movement. Temporal comparison of two-wavelength multiplexed hologram has been used for calculations. The radius value was calculated from the information of the vein shape, obtained by means of double wavelength holography, while the deformation of the vein has been measured with traditional holographic interferometry. In this work, both techniques have been combined using only one recording system.

The technique has been tested in a latex tube and in a sheep aorta (ex-vivo). The experiments in both cases have been designed to simulate real patient situations. Differences found between the model and real vessels are presented in the paper.

Highlights:

Simultaneous shape and deformation measurements in blood vessels (ex-vivo) using off-axis holography.

Compact digital holography setup to measure 3D information with only one camera.

Dual wavelength holography applied to measure the shape of biological tissues.

Keywords: Digital holography, Dual wavelength holography, Radial deformation of blood vessels, Shape of veins.

1. Introduction

Cardiovascular diseases are the leading cause of death or disability in the population of developed countries. Experts from multiple disciplines work to improve the diagnosis, prevention and treatment of these conditions. There is an increasing interest in the experimental measurements of blood flows, as well as the deformation of vein walls, in the study of cardiovascular diseases. For biomedical applications, optical non-intrusive techniques such as digital holography [1] are very suitable due to their non-contact character.

An area of interest is the measurement of the velocity fields inside the blood vessels. Holographic techniques have been widely applied to measure velocity fields in confined liquid flows with complex geometry recording configurations [2-3]. As real veins are opaque a transparent vein model was required. In those cases the liquid was enclosed in a transparent vessel, allowing observation through transparent windows [4]. Direct visualization can also be done through the use of endoscopes designed for this inspection [5]. With this setup is even possible to measure simultaneously the velocity flow and the inner wall deformation but only in a small area.

There is also a growing interest in the experimental study of blood vessels ‘wall deformation. Numerical simulations of the vein behavior based on *In-Vivo* data obtained from ultrasonic or tomographic techniques have been developed [6-7]. Nevertheless, it is interesting to investigate other techniques to measure in vitro the deformation of veins with possibilities to apply in-vivo lately. For blood vessels one of the most interesting parameters is radial deformation, as it could be easily be related to defects in vein tissue. The radial deformation of the veins can be calculated using the out of plane deformation and the radius value, which can be obtained from the knowledge of the shape.

For a real patient, the main veins and arteries diameters go approximately from 7.5 mm to 20 mm. Due to the cardiac movement, they suffer micrometrics deformations that in some cases reach up to millimeters. The different order of magnitude of the radius and the deformation limits the techniques that can be applied to obtain both magnitudes at the same time.

Digital holographic techniques have been investigated due to the high sensitivity and because endoscopic holography is a promising technique for the future in-vivo application. Digital Speckle Pattern Interferometry (DSPI) has been applied to measure small deformations in a wide range of objects retrieving different components depending on the recording geometry [8-9]. This digital holographic interferometry allows a comparison of wavefronts recorded at different times. The numerical reconstruction of the holograms is calculated and compared to obtain a 2-D deformation map [10].

Digital Dual wavelength holography was introduced as a shape measurement technique of solid objects by Pedrini et al [11-12] and Wagner et al. [13-14]. It requires the recording of two holograms with different wavelengths. The comparison of the numerical reconstruction of the hologram for each wavelength gives information about the object shape. The use of two wavelengths has some drawbacks in the reconstruction process, such as the different object size and image plane location. Then, several methods have been proposed to compensate this chromatic aberration avoiding incorrect superposition [15-17]. The technique was initially applied to obtain the contour map of large solid objects. Lately it has been applied to measure the shape of microscopic samples and many efforts have been done on the developing of new optical setups or algorithms to remove the phase ambiguity [18-21]. A simultaneous recording of both wavelengths was proposed for the first time by Kühn et al. [19] by multiplexing the information using two reference beams, one for each wavelength. Then, the two off-axis holograms were recorded simultaneously on the camera. Other different setups for multiplexing have been investigated in the past recent years [22-25].

Different holographic recording systems have been proposed to measure shape and deformation at the same time, but several cameras are needed, resulting in more complicates setups [26-28]. In this paper, an off-axis holographic setup with only one camera for the simultaneous measurement of the deformation and shape is presented. The technique has been applied in blood vessels (biological tissue ex-vivo) to obtain the radial deformation.

Temporal series of multiplexed holograms are recorded. In each hologram the information from the two wavelengths are recorded separately. For any hologram, using the information of the two wavelengths, it can be retrieved the shape and calculate the vein radius. By comparing the information for one of the two wavelengths obtained from two successive holograms, micrometric deformations can obtained. Both magnitudes are combined to calculate a 2D map of the radial deformation.

For large deformations the shape measurements obtained from the two-wavelength technique can be also used to obtain the 2D deformation map. However, the optical path length differences measured with Holographic Interferometry techniques depends of the observable fringes in the phase difference map. Thus, to measure the shape of human veins a synthetic wavelength in the millimeters range is required while a wavelength below the micron is needed to measure micrometric deformations. On the other hand, the sensitivity of the one-wavelength technique allows measuring deformations in the micron range, and therefore its temporal evolution up to the range of millimeters, as it will be explained below.

To validate the technique, it has been applied to measure the shape and the radial deformation of a latex tube, considered as a simplified blood vessel and on a real sheep aorta. A versatile and simple setup, with beams guided by fiber optics and small angles in the recording, has been designed to make possible, in the future, the application for in-vivo medical inspection using endoscopes [5] or similar devices designed for this purpose.

2. Digital Image Holography

In digital image holography [1] an object is illuminated and its image (the object wave o(x,y)) is formed with a lens on a digital sensor. There, it interferes with a reference wave, r(x,y), that comes from the same laser source. Thus, the recorded hologram is an image hologram of the object. The object and reference complex waves can be written as:

$$o(x,y) = A_o(x,y)\exp\left[j\phi_o(x,y)\right]$$
$$r(x,y) = A_r(x,y)\exp\left[j\phi_r(x,y)\right] \quad (1)$$

where A is the wave amplitude and ϕ the phase. The hologram intensity is given by:

$$I(x,y) = |o(x,y)|^2 + |r(x,y)|^2 + r^*(x,y)o(x,y) + r(x,y)o^*(x,y) \quad (2)$$

The first two terms are the dc term, the third and fourth terms correspond to the real and virtual image. The equation can also be written as:

$$I(x,y) = (A_o(x,y))^2 + (A_r(x,y))^2 + 2A_o(x,y)A_r(x,y)\cos(\phi_o(x,y) - \phi_r(x,y)) \quad (3)$$

showing that the information of the amplitude and the phase of the object wave is recorded in the hologram.

Due to the resolution of the camera sensor, a small angle between the two beams is required to record an off-axis hologram. Then a cube beam splitter is place in front of the camera to combine both beams and ensure the appropriate small angle between them. If the source of the divergent reference beam is located at the same distance from the sensor as the lens aperture used to image the object a lensless Fourier Transform hologram is recorded (Fig. 1).

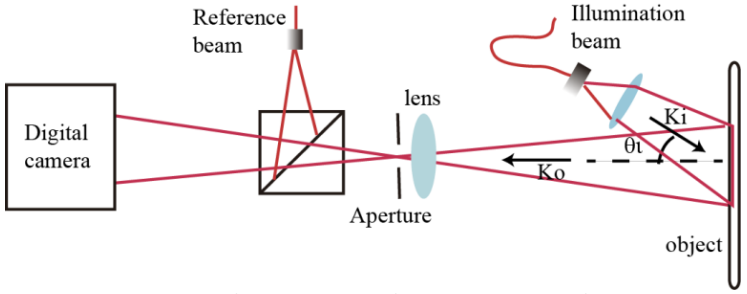

Fig. 1. Optical setup for the recording of a Fourier Lens less of the aperture

The isolation of the real image from the virtual image and the dc term is difficult. However, by introducing a spatial phase shifting (SPS) the isolation in the frequency domain is possible [29]. To introduce a linear phase shifting the origin of the reference wave is displaced an amount Δr from the lens aperture center (Fig. 2a). To resolve this modulation frequency, the lens aperture has to be reduced to increase the speckle size appropriately up to a value of around three pixels [30]. In this case, the Fourier Transform of the digital hologram (Fig. 2b) shows the real and virtual images of the lens aperture centered at a frequency $\pm f_o$ proportional to the reference beam displacement Δr. The dc term appears as a bright spot on the center.

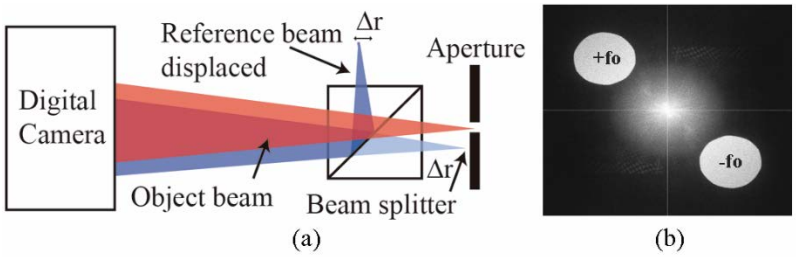

Fig. 2. a) Object and reference beam combination setup. b) Fourier plane showing the aperture real and virtual image

The separation of these two images of the lens aperture allows selecting only one of them for the reconstruction process while the rest is blocked [31]. Then, the complex amplitude distribution is propagated to the object plane, where the intensity and phase distribution is reconstructed. The numerical reconstruction can be done using the Fresnel approximation [32] or the Fourier Transform method [33].

The comparison of two complex amplitudes gives a wrapped phase difference map (modulo 2π). Low pass filter and phase unwrapping processes are applied in order to obtain quantitative information of the phase change at any point, $\Delta\phi(x,y)$. The unwrapping process gives an extended value of the phase change out of 2π, but an external reference is required to know the absolute phase value. The accuracy in the phase recovered is

determined by the SPS technique and, in general, is accepted as a fringe/50, i.e. roughly as λ/100. When the final phase is calculated by adding several phase values the final accuracy is expected to be lower.

The comparison of object waves corresponding to different wavelengths gives information of the shape. When comparing object waves recorded at different time instant information of the object deformation is retrieved.

2.1 Deformation

The comparison of the object complex amplitudes obtained at two different time instants allows retrieving information about the object deformation [34]. The sensibility of the technique is related to the recording geometry given by the illumination and observation direction. The illumination direction, k_i, is determined by the direction of the laser beam used to illuminate the object. The observation direction, k_o, is the direction of the light scattered by the object surface to the camera. The sensitivity vector, K, is defined as $K= (k_o-k_i)$ (Fig.1).

The phase change at any position, $\Delta\phi(x,y)$, is related to the displacement in the sensitivity direction by the next equation:

$$\Delta\phi(x,y) = \vec{K}\cdot\vec{L} \tag{4}$$

For situations with out of plane deformations mainly, the phase change at any point $\Delta\phi(x,y)$, is related with $L_k(x,y)$ by the following equation;

$$\Delta\phi(x,y) = \frac{2\pi}{\lambda}\left(\cos\theta_i + \cos\theta_o\right)L_K(x,y) \tag{5}$$

being θ_i and θ_o the angles between the optical axis and the illumination and observation directions respectively. Both angles, θ_i and θ_o, are very small and can be set to zero, which make this configuration very suitable for future applications with endoscopes.

The technique gives the relative phase change in all points of the surface. The phase maps in these techniques present a global unknown phase change due to random variations in the air over the path length during the recording process. A still area in the object is required to know the absolute phase value and ensure an accurate comparison.

2.2. Shape

Information about the object shape can be obtained from the comparison of the object complex amplitudes recorded with different wavelength. In this case, the phase difference map is related to a new wavelength Λ, called synthetic wavelength, given by the following equation:

$$\Lambda = \frac{\lambda_1\lambda_2}{\lambda_2 - \lambda_1} \tag{6}$$

The phase difference at any point is related to the local surface height, Z(x,y) according to this equation:

$$\Delta\phi(x,y) = \frac{2\pi}{\Lambda}\left(\cos\theta_i + \cos\theta_o\right)Z(x,y) \tag{7}$$

To introduce a referential for the surface height, the phase difference map at a plane Z=0 is obtained and used as a background to subtract to any phase difference map. Thus, the Z(x,y) value obtained is referred to this plane. When the Fresnel algorithm is used for reconstruction the background is calculated at the Z=0 position. When the numerical reconstruction is done with the Fourier Transform method, the phase background is obtained from a hologram of a plane surface located at Z=0 previously recorded [35].

3. Simultaneous shape and deformation optical setup

To record the deformations and shape simultaneously, dual wavelength holograms will be recorded at each object state. The scheme of the optical setup used for the recording is shown in figure 3a. Two solid state lasers (Cobolt Flamenco) with fixed nominal wavelengths of λ_1=659.597 nm and λ_2=659.477 nm have been used. The synthetic wavelength value is Λ=3.6 mm. The reference and object beams are obtained by dividing the laser beam and guided through optical fibers. As both wavelengths have a very close value the chromatic aberration can be disregarded.

The two object beams, guided by optical fiber, are combined by means of a 2x2 single mode Fused Fiber Optic coupler (FC632-50B-FC) to ensure a common optical path and the same collimated illumination direction for both wavelengths. The object is illuminated at an angle $\theta_i \approx 7^o$ with the optical axis. The light scattered by the surface (object beam) is imaged onto a digital camera by a 125 mm focal length converging lens. The camera (SCMOS PCO edge) has a 2160 x 2560 pixels sensor, with a pixel size of 6.5μm. The camera sensor is placed perpendicular to the optical axis ($\theta_o \approx 0^o$) at a distance to the aperture plane, about 250 mm. In the setup, the object distance is a=233 mm and the image distance is a'=265 mm, given a magnification value M=0.88.

The optical fiber ends of both references are at the same distance from the sensor as the lens aperture to record a lensless Fourier hologram of the aperture. The multiplexing is obtained just by displacing the divergent reference wave origin in different direction for each wavelength. The appropriate location of the fiber optic tips produces the correct multiplexing. Then, the two aperture images for each wavelength are located at a different quadrant in the Fourier plane (Fig. 3b).

A cube beam splitter (50/50) is place in front of the camera to combine the object and the reference beams. Then, the small angle required between them, due to the low spatial resolution of the CMOS sensors, is ensured.

Typically in interferometric techniques a random global phase may appear in the difference phase map. To remove this random phase a reference position without or with known displacement within the field of view is required. In our experiments, a small flat piece of metal plate parallel to the camera was place at the bottom of the image in all recorded holograms and used as a referential for temporal comparison. Then, the mean phase value in the metal piece area is subtracted in all filtered phase difference maps to eliminate the random phase and ensure the same phase reference in all difference phase maps.

The object complex amplitudes are reconstructed using a Fresnel propagation algorithm and the appropriate aperture image is selected. To determine accurately the referential plane Z=0, the propagation algorithm is iteratively applied to different planes, around the referential plane position, until the phase in the metal plate area is almost constant. Then, the object distance, a, can be determined with an accuracy of 0.1 mm. The phase difference map corresponding to this plane position is calculated from the recording geometry parameters and used as background.

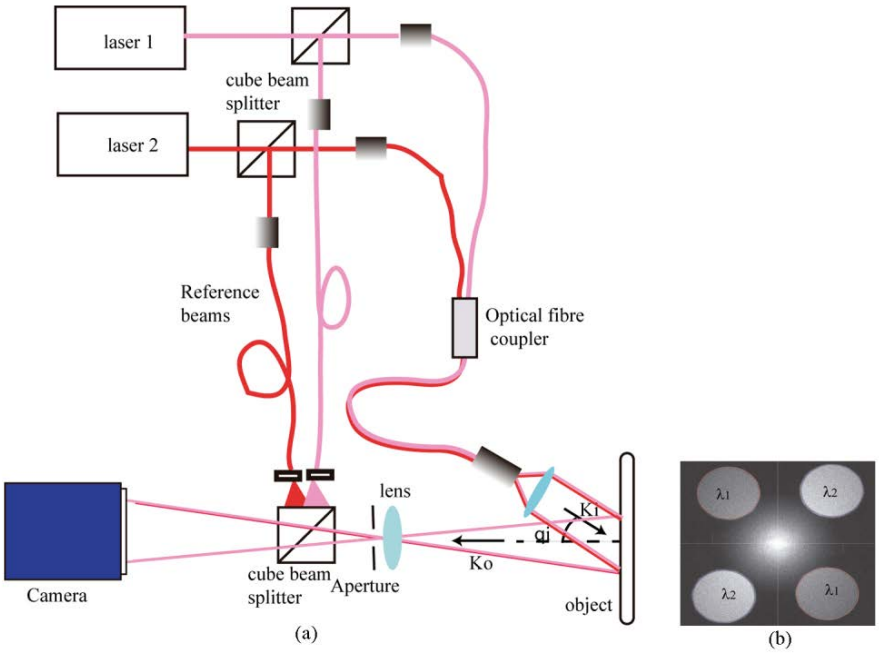

Fig. 3. a) Optical setup for recording two multiplexed holograms. b) Fourier plane of the multiplexed recorded holograms.

4. Results in a cylindrical latex tube

Firstly, the technique has been tested in a latex tube, considered as a simply blood vessel model. The tube, held by its ends, was filled with a mixture of water and glycerol (ρ= 1.15 g/cm^3), and connected to an external

reservoir. Changes in the height of the liquid reservoir generated changes in the inner tube pressure according to the Bernoulli laws. In our case the relation is ΔP (mmHg) = 0.085 Δh (mm). As the height of the reservoir is measured with an accuracy of 0.5 mm ($\sigma_{\Delta h}$=0.5 mm), then $\sigma_{\Delta P}$=0.0425 mm Hg. Dual wavelength multiplexed holograms were taken for different states corresponding to different inner pressure in the tube.

A latex tube with an external diameter of 12.33 mm has been used in these experiments. To increase the light scattered by the object, ZnO powder has been applied to the surface. Care was taken to place the tube horizontal and parallel to the camera sensor to simplify calculations. The piece of a metal flat surface placed below the tube is used to have a common phase referential in all recordings (Fig. 4a). From the focused image of the scale (Fig. 4b) the recorded area in all images (19 mm x 16 mm) and the magnification have been determined. An image of the scale wrapped around the tube (Fig. 4c) shows that the recorded length over the tube is 16 mm, which corresponds to the 40% of the total perimeter. The magnification is the same in all the experiments presented in this paper.

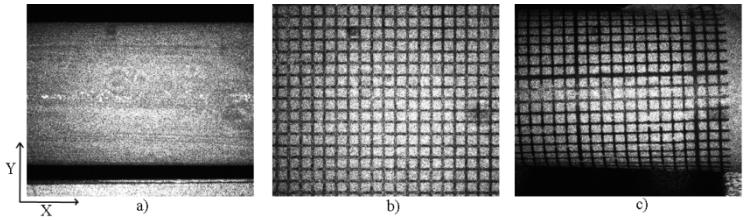

Fig. 4. Measurements in a latex tube. a) Image of the tube. b) Millimeter scale at the reference plane. c) Millimeter scale wrapped over the tube.

Comparing the reconstructed complex amplitude obtained for each wavelength, the shape information is obtained. The phase difference map obtained is shown in figure 5a. After a low pass filtering process the image is multiplied by an appropriate mask to isolate the tube area (Fig. 5b). The mask is obtained from the image of the object and narrowed up to 6 pixels in the edges to eliminate the fails due to the filtering process. The unwrapped phase is used to calculate the height of any object point, Z(x,y), according to equation 7. The 3D representation is presented in figure 5c.

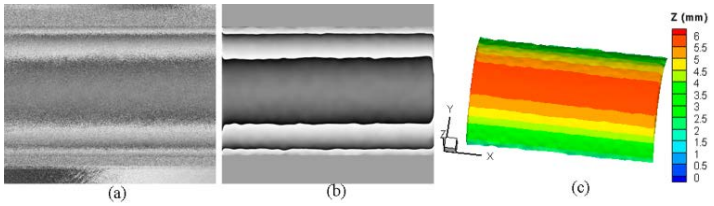

Fig. 5. Shape measurements. a) Difference phase map b) Filtered phase map with mask c) 3D shape map.

According to the established accuracy for this technique, our precision for the Z measurement should be 0.036 mm. But since the fringes are not equally spaced the analysis process introduces more errors resulting in lower final precision.

Given a cylindrical shape of the tube, the Z data for each column (X) are fitted to a circumference, which gives its radius and center values (Fig.6). Although small fluctuations appear due to the noise in the image, the obtained mean radius is 6.217 and the calculated center is at Y_c= 7.9 mm and at a Z_c = 6.4 mm. The radius value is in very good agreement with the measured value with a gage that is 6.17 mm. The diameter discrepancy is associated to the small deformation of the tube during the measurement process with a Vernier caliper.

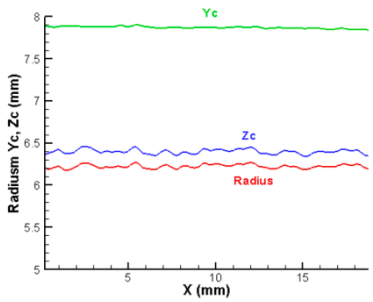

Fig. 6. Radius and center position results

Changes in the reservoir height introduced changes in tube. Holograms were recorded for different pressures by changing the reservoir height every 5 mm up to a value of 50 mm. This corresponds to pressure changes of 0.425 mmHg up to a total of 4.25 mmHg. The comparison of the complex amplitude obtained for the same wavelength but at different states is related to the deformation of the tube with the pressure change. As we have recorded hologram series, the comparison corresponding between any different surface states can be performed. Three examples of phase difference maps are shown in figure 7.

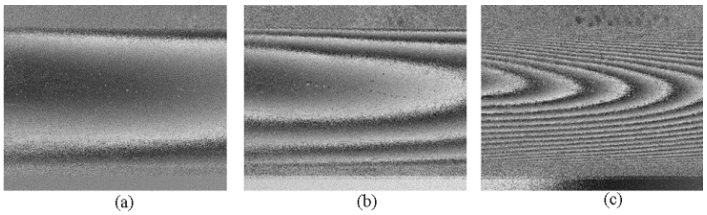

Fig. 7. Deformation in a latex tube. Difference phase maps for a) ΔP=0.425 mmHg. b) ΔP=0.85 mmHg. c) ΔP= 4.25 mmHg.

The surface displacement Lz(x,y) is retrieved from the unwrapped phase change $\Delta\phi(x,y)$ according to equation 5. For high deformations (Fig. 7c) the fringes cannot be resolved. Thus, the corresponding final displacement field must be calculated by adding the displacement fields obtained for smaller pressure changes corresponding to phase difference maps with well resolved fringes. The nature of the fringe pattern for cylindrical objects, with very close fringes in the edges, introduces errors in these areas. Then, for calculations, difference phase maps corresponding to steps of ΔP=0.425 mmHg, with less fringes in the edges, have been used instead of those corresponding to steps of ΔP=0.85 mmHg.

The object is far enough from the camera to consider K value constant for all points in the image. The combination of Lz(x,y) with the radius and centre position information, determined from the shape measurement, the radial deformation can be calculated. Results obtained for the step of ΔP=0.425 mmHg are presented in figure 8. The maximum deformation in the out of plane direction measured is of 0.8 μm. If the tube is centred, the out of plane and the radial component in the centre of the tube should have the same value. Although the radial displacement was expected to be constant variations smaller than 0.1μm have been measured (fig 8 c). These variations are caused by our tube holding system that allows small movements.

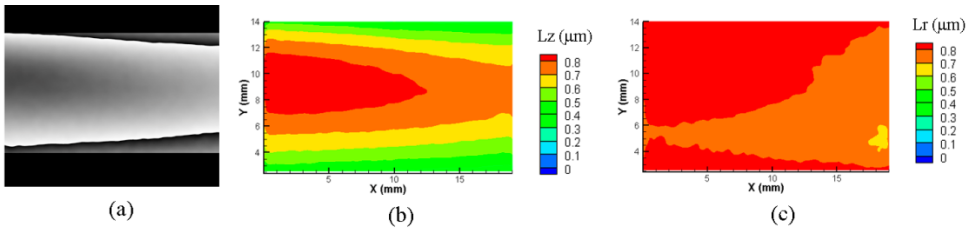

Fig. 8. Deformation of a latex tube for ΔP=0.425 mmHg. a) Filtered difference phase map b) Lz, displacement in the out of plane direction c) Lr, radial displacement.

The final deformation for ΔP=4.25 mmHg has been calculated adding the deformation retrieved for any ΔP=0.425 mmHg. To ensure the same phase reference in all phase difference maps, the mean phase value in the metal plate recorded at the bottom is subtracted to the filtered phase difference maps for calculations. A maximum out of plane displacement of 12 μm has been obtained at the center of the tube (Figure 9). Then, a radial displacement close to this value is obtained in the central part of the tube. It is observed up to a 10% radial deformation change along the X direction as in any step used for calculation.

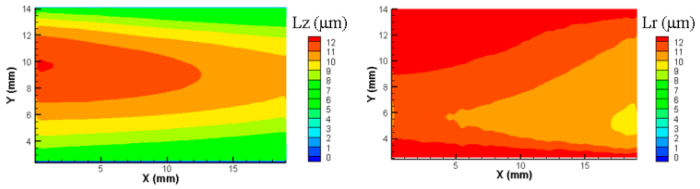

Fig. 9. Deformation of the latex tube at the final state (ΔP= 4.25 mmHg). a) final out of plane displacement, Lz b) final Radial-displacement, Lr

5. Results in a sheep aorta

The same experiments performed with the tube were carried out in a sheep aorta (Fig. 10). As this procedure dries the surface changing the elastic properties, a different piece of 5cm length of artery was used in every experiment. The surface was covered with ZnO powder to increase the scattered light. The recording process is done with the artery in air held by two glass tubes introduced in its ends. Despite the holding system no significant movements were detected during the recording process.

Fig. 10. Image of the total length sheep aorta used.

The artery surface is completely different from the tube and presents some protuberances due to the tissue nature which result in shadow areas. Dual wavelength holograms of the artery were recorded. In addition, the object illuminated with white light was recorded.

The same analysis procedure as for the tube was done. A filtered process, a mask to isolate the area and an unwrapping process was applied to phase difference maps to retrieve the shape information (Fig. 11). The mask was calculated using the white light image of the artery. Let us remark that the holes, vein folders or areas with no light introduce errors and no real information is retrieved.

Different side views of the artery were recorded, just rotating it. Some images, presenting different surface peculiarities and the measured shape are presented in figure 11 and 12. In figure 11 the protuberances in the lower part introduced some shadows that caused errors in the analysis. In figure 12 the areas with the tissue coming out can be observed in the phase map and are reported on the results. In general a good agreement in the shape measurements was obtained. In the positions with big protuberances the radius value is not determined with precision. However, an accurate mean radius value can be retrieved.

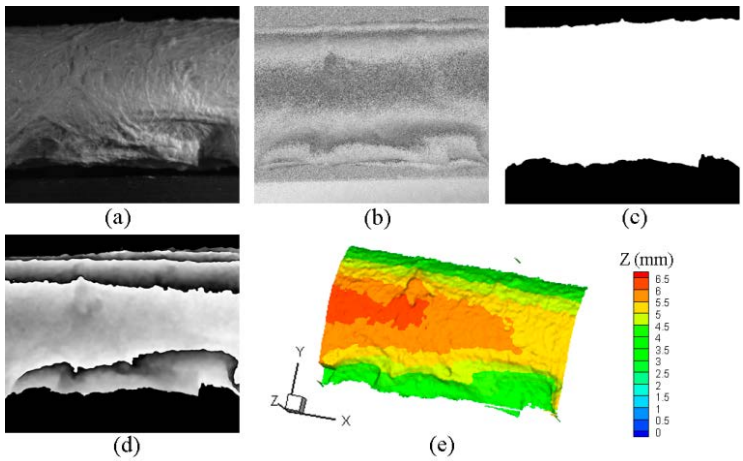

Fig. 11. A side view of the artery for shape measurements. a) Image recorded with white light b) phase map c) mask. d) Filtered phase map with mask e) 3D shape representation.

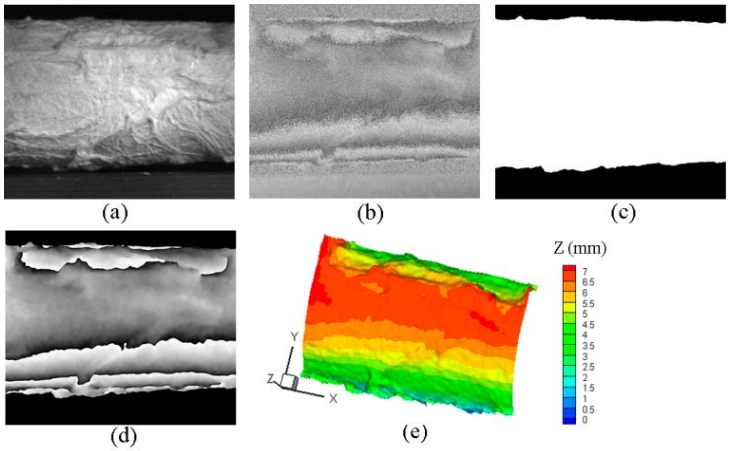

Fig. 12. A side view of the artery for shape measurements. a) Image recorded with white light b) phase map c) mask. d) Filtered phase map with mask e) 3D shape representation.

The following experiment was carried out to measure the shape and the deformation of the sheep aorta. In this experiment, a different piece of aorta, with a non-constant diameter in this case, was placed horizontally. As in the previous experiment, changes in the reservoir height gave changes in the artery inner pressure. Dual holograms were recorded for each position of the liquid reservoir.

The shape is retrieved comparing the object wave recorded with both wavelengths. The analysis of these phase difference maps allow calculating the Z value of any surface point from to the referential plane (Z=0). Results are presented in figure 13.

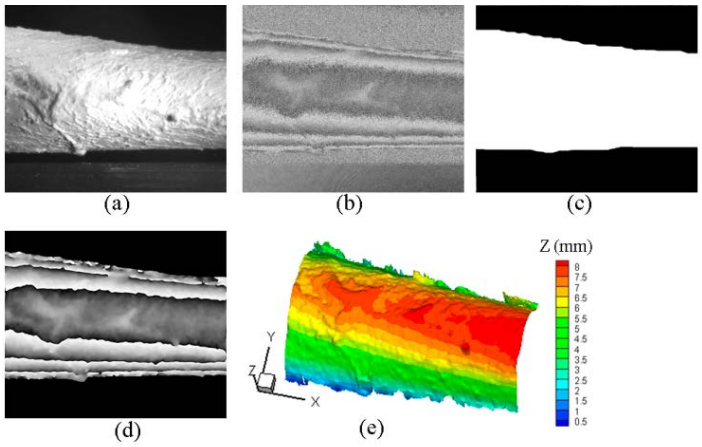

Fig. 13. Artery shape measurements. a) Image recorded with white light b) Difference phase map. c) Filtered phase map with mask d) 3D phase map.

A radius value is obtained using the assumption that for any X position the shape along the vertical axis can be considered a circumference (Fig. 14). The external features in the tissue, which can be seen in the white light image, correspond to the peaks in the radius value. Besides, shadows in the edges due to small vein folds also introduce errors in the radius values. Nevertheless, the radius tendency is well determined.

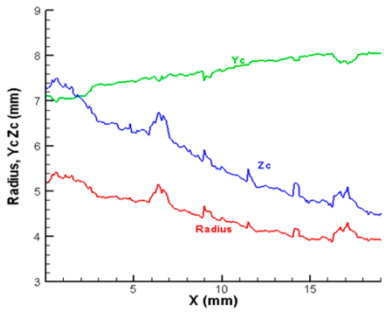

Fig. 14. Fitted value for the radius and center of the circumference.

Now, the artery deformation will be presented. Since the artery is less rigid than the tube, greater deformation was expected for the same pressure changes. Figure 15a shows that the aorta deformation for a pressure difference of only 0.085 mmHg (reservoir height change Δh=1 mm) is too big to be measured directly. For this reason, several holograms with smaller pressure changes were recorded, so that the fringes could be resolved on each phase difference maps (Fig. 15b, c).

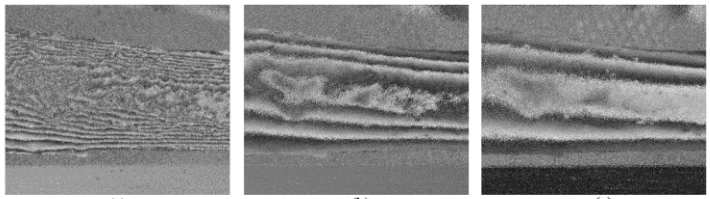

Fig. 15. Differnce phase maps corresponding to deformation of a piece of artery of different changes in height. a) Δh=1mm b) c) two of the seven states recorded up to a Δh =1 mm.

In our case, seven holograms were recorded with a final Δh=1 mm. Adding the deformation obtained for any of these holograms the final displacement for 0.085 mmHg is obtained (Fig. 16).

The fitted radius value is used to calculate the radial deformation. A maximum value around 7 μm has been measured. Errors close to the edges are observed due to a small fold on the upper surface.

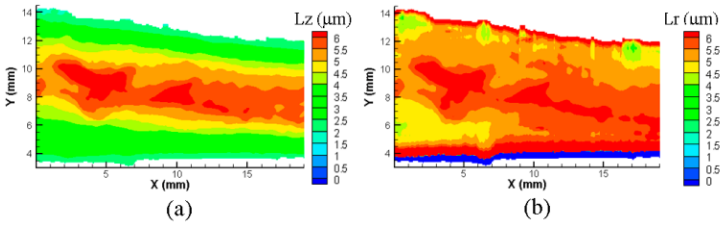

Fig. 16. Total deformation of a sheep aorta for ΔP=0.085 mmHg: a) out of plane and b) radial deformation map.

Although the accuracy decrease when the addition of deformation maps is required, this procedure allows to study a wider range of displacements, and therefore, to study the real tissue behavior. Since series of hundreds or thousands holograms can be easily recorded with this setup, bigger final deformations could be measured.

6. Conclusions

In this paper a method for measuring simultaneously the shape and the deformation of a blood vessel model is presented. The different order of magnitude of both lengths makes this measurement difficult. A setup with just one camera has been used. It has been applied on a tube, with cylindrical shape and on a real sheep aorta (ex-vivo). A setup to change the inner pressure has been designed to generate micrometric deformations in the blood vessels.

Series of multiplexed dual wavelength holograms were recorded for different inner pressures. The multiplexing allows recovering separately the information from each wavelength. The shape surface has been calculated using the Fresnel approximation and the data for any transversal section were fitted to a circumference to determine the radius and center position. The temporal comparison of the object complex amplitude gave information on surface change along the sensitivity vector direction. Using the previously measured radius, the radial deformation was calculated.

The radial deformation has been measured in a latex tube whose external diameter is 12.33 mm. The displacement field for a total pressure change of 4.25 mmHg has been calculated by adding the displacement fields corresponding to consecutive holograms with a pressure change of 0.425 mm Hg. A radial deformation of 12 μm has been measured with a variation along the horizontal direction smaller than 1 μm due to the holding setup.

The technique has been applied to a real sheep aorta. The 3D shape maps obtained show a good agreement with the white light image recorded giving information about the external features. The deformation and shape has been measured simultaneously in a piece of artery with a non-constant radius. The external radius goes between 5.2 mm to 4 mm. The final displacement for ΔP=0.085 mmHg has been calculated using intermediate states. A radial displacement value around 7.0 μm, not uniform along the surface has been measured. Results had shown the different behavior of a tube and the real blood vessel. Bigger deformations can be measured recording a higher number or digital holograms. A high speed camera could be used for dynamic situations.

The knowledge of the radial deformation, independent of the specific recording geometry, can be related with defects on the vessel walls or with different pathologies. The simplicity of the setup makes it possible to be implemented as a holographic endoscope or similar device and applied to in-vivo measurement.

7. Funding and acknowledgments

Spanish Ministerio de Economía y Competitividad (MINECO) and European Commission FEDER program (project DPI2016-75791-C2-2-P/1-P); Gobierno de Aragón (Laser Optical Technology - E44-17R- research group)

Authors would like to acknowledge the use of Servicio General de Apoyo a la Investigación-SAI, Universidad de Zaragoza.

References

1. U. Schnars and W. Jueptner, “Digital Holography: Digital Hologram Recording, Numerical Reconstruction and Related Techniques, Berlin, Germany: Springer 2005.
2. N. Andrés, M.P. Arroyo, H. Hinrichs and M. Quintanilla. “Digital speckle interferometry as a full-field fluid-velocity technique,” *Opt. Lett.*, vol. 24, no. 9, pp. 575–577, May 1999.
3. V.R. Palero, J. Lobera and M.P. Arroyo. “Three-component velocity field measurement in confined liquid flows with high-speed digital image plane holography,” *Exp. Fluids.*, vol. 49, no. 2, pp. 471–483, Aug. 2010.
4. L. Arévalo, E. Roche, V. Palero, M.A. Martinez and M.P. Arroyo. “PIV and digital holography for measuring blood flows and vessel wall dynamics,” *in Proc. SPIE. 8785* Porto, Portugal 2013, 8785CY.
5. L. Arévalo, V. Palero, J. Lobera, N. Andrés and M.P. Arroyo. “Combining endoscopes with PIV and digital holography for the study of vessel model mechanics,” *Meas. Sci. Technol.*, vol. 26, no. 11, pp. 115701-115701, Sep. 2015.
6. A. Swillens, G. De Santis, J. Degroote, L. Lowstakken, J. Vierendeels and P. Segers. “Accuracy of carotid strain estimates from ultrasonics wall tracking: A study based on multiphysics simulations and In Vivo Data,” *IEEE Trans* Med Imaging. Vol 31, no. 1, pp. 131-139, Jan. 2012.
7. G. Choi, G. Xiong, C.P. Cheng and C.A. Taylor. “ Methods for characterizing human coronary artery deformation from cardiac-gated computed tomography data,” *IEEE Trans Biomed Eng*., vol. 61, no. 10, pp. 2582-2592, Oct. 2014
8. P.K.Rastogi (Ed), “Digital Speckle-Pattern Interferometry and related techniques,” Chichester, U.K Wiley, 2001.
9. T. Kreis, “Handbook of Holographic Interferometry: Optical and Digital Methods”, Wiley-VCH Verlag GmbH, 2005.
10. S. Recuero, N. Andrés, J. Lobera, M. P. Arroyo, L. A. Angurel and F. Lera, 2Application of DSPI to Detect Inhomogeneous Heating on Superconducting Ceramics. *Meas. Sci. Technol*, vol 16, no 4, pp. 1030-1036, Mar 2005.
11. G. Pedrini, P. Fróning, H.J. Tiziani and M.E. Gusev. “Pulsed digital holography for high-speed contouring that uses a two-wavelength method,” *Appl. Opt*., vol. 38, no. 34, pp. 7056-7062, Jan. 1999.
12. G. Pedrini, H.J. Tiziani, M.E. Gusev. “Pulsed digital holographic interferometry with 694- and 347- nm wavelengths,” *Appl. Opt.*, vol. 39, no. 2 pp. 246-249, Feb. 2000.
13. C. Wagner, S. Seebacher, W. Osten, W. Júptner. “Digital recording and numerical reconstruction of lensless Fourier holograms in optical metrology” *Appl. Opt*., vol. 38, no. 22, pp. 4812-4820, May. 1999.
14. C. Wagner, W. Osten, S. Seebacher. “Direct shape measurement by digital wavefront reconstruction and multiwavelength contouring,” *Opt. Eng.*, vol. 39, no. 1, pp: 79–85, Jan 2000.

15. P. Ferraro, S. De Nicola, G. Coppola, A.Finizio, D. Alfieri and G. Pierattini. “Controlling image size as a function of distance and wavelength in Fresnel-transform reconstruction of digital holograms,” *Opt. Lett.*, vol. 29, no. 8, pp; 854-856, Apr 2004.
16. S. de Nicola, A.Finizio, G. Pierattini, D. Alfieri, S. Grilli, L. Sansone and P. Ferraro,. “Recovering correct phase information in multiwavelength digital holographic microscopy by compensation for chromatic aberrations” *Opt. Lett.*, vol. 30, no. 20, pp; 2706-2708, Oct 2005.
17. P. Ferraro, L. Miccio, S. Grilli, M. Paturzo, S. De Nicola, A.Finizio, R. Osellame and P. Laporta. “Quantitative Phase Microscopy of microstructures with extended measurement range and correction of chromatic aberrations by multiwavelength digital holography,” *Optics Express*, vol. 15, no. 22, pp; 14591-14600, Oct 2007.
18. D. Parshall, K.M. Kim. “Digital holographic microscopy with dual-wavelength phase unwrapping,” *Appl. Opt*., vol. 45, no. pp: 451-459, Jul. 2006.
19. J. Kühn, T. Colomb, F. Montfort, F. Charrière, Y. Emery, E. Cuche, P. Marquet and C. Depeursinge. “Real-time dual-wavelength digital holographic microscopy with a single hologram acquisition,” *Optics Express*, vol. 15, no. 12, pp; 7231-7242, May 2007.
20. P. Bergstrom, S. Rosendahl, P. Gren and M. Sjodahl. “Shape verification using dual-wavelength holographic interferometry,” *Opt. Eng*., vol.50, no. 10, pp: 101503-1-7, Oct. 2011.
21. Z. Wang, J. Jiao, W. Qu, F. Yang, H. Li, A. Tian and A. Asundi.”Linear programming phase unwrapping for dual-wavelength digital holography,” *Appl. Opt*., vol. 56, no.3 ,pp: 424-433, Jan. 2017.
22. T. Saucedo, F. Mendoza, M. De la Torre, G. Pedrini. and W. Osten. “Simultaneous two-dimensional endoscopic pulsed digital holography for evaluation of dynamic displacements,” *Appl. Opt*., vol. 45, no. 19, pp: 4534-4539, Jan. 2006.
23. P. Bergstrom, D. Khodadad, E. Hallstong, M. Sjodahl. “Dual-wavelength digital holography: single-shot shape evaluation using speckle displacements and regularization,” *Appl. Opt*., vol. 53, no. 1, pp: 123-131, Jan. 2014.
24. Z. Wang, Z. Jiang and Y. Chen. ”Single-shot dual-wavelength phase reconstruction in off-axis digital holography with polarization-multiplexing transmission,” *Appl. Opt*., vol. 55, no. 22, pp: 6072-6078, Jul. 2016.
25. N.A. Turko and N. T. Shaked, “Simultaneous two-wavelength phase unwrapping using an external module for multiplexing off-axis holography.” *Opt. Lett.*, vol. 42, no. 1, pp: 73-76, Nov. 2017.
26. M. Dekiff, P. Berssenbrügge, B. Kemper, C. Denz and D. Dirksen. “Simultaneous acquisition of 3D shape and deformation by combination of interferometric and correlation-based laser speckle metrology,” *Biomed. Opt. Express*., vol. 6, no. 12, pp: 4825–4840, Oct. 2015.
27. S. Seebacher, W. Osten, W. Júptner. “Measuring shape and deformation of small objects using digital holography,” in Proc. SPIE 3479, San Diego, CA, United States 1998, 104-115.
28. T. Hansel, R. Grunwald, K. Reimann, J. Bonitz, C. Kaufmann, and U. Griebner. “Deformation Measurements of High-Speed MEMS With Combined Two-Wavelength Single-Pulse Digital Holography and Single Phase Reconstruction Using Subpicosecond Pulses,” *IEEE Journal of selected topics in quantum electronics.* Vol 15, no. 5, pp. 1351-1358, Sept. 2009.
29. J. Lobera, N. Andrés, M.P. Arroyo, “Digital speckle pattern Interferometry as a holographic velocimetry technique,” *Meas. Sci. Technol*., vol. 15, no. 4, pp: 718-724, Mar. 2004.
30. J. Burke, H. Helmers, C. Kunze, and V. Wilkens, “Speckle intensity and phase gradients: influence on fringe quality in spatial phase shifting ESPI systems,” Opt. Commun. 152, 144–152 (1998).
31. E. Cuche, P. Marquet and C. Depeursinge. “Spatial filtering for zero-order and twin-image elimination in digital off-axis holography,” *Appl. Opt*., vol. 39, no. 23, pp: 4070–5, May 2000.
32. J.W. Goodman. “Introduction to Fourier Optics,” New Y o r k , NY, USA: McGraw-Hill, 1968.
33. M. Takeda, H. Ina, S. Kobayashi, “Fourier-transform method of fringe-pattern analysis for computer based topography and Interferometry,” *J. Opt Soc. Am.*, vol. 72, no. 1, pp: 156-160, Aug. 1982.
34. C.M. Vest, “Holographic Interferometry,” New York, NY, USA: Wiley, 1979.
35. Andrés, N.; Pinto, C.; Lobera, J.; Palero, V.; Arroyo, M.P. Simultaneous shape and deformation measurements in a blood vessel model by two wavelength interferometry. Proceedings SPIE 10333 in Optical Methods for Inspection, Characterization, and Imaging of Biomaterials, I1-I8. June 2017.